Surface trapping during hyperthermal energy scattering

A. C. Lavery, C. E. Sosolik, and B. H. Cooper*
Laboratory of Atomic and Solid State Physics, Cornell University, Ithaca, New York 14853-2501
(Received 30 May 2000)

We present the results of a detailed investigation of surface trapping during the scattering of hyperthermal ($\leqslant$600 eV) energy ions from metallic surfaces. Recent experiments have revealed that trends in surface trapping probabilities are highly dependent on factors such as incident ion energy, species, and angle. By comparing the results of classical trajectory simulations to experimental data, we show that the *surface corrugation* seen by the incident ions plays a key role in determining surface trapping trends for ions incident at hyperthermal energies.

I. INTRODUCTION

The fate of a hyperthermal energy ion scattering from a metallic surface is determined by many factors, including the incident ion energy and species, the surface structure and composition, and the incident angle. If an incident ion loses sufficient energy during inelastic collisions with surface atoms it may become trapped in the attractive potential well at the surface. Alternatively, the incident ion may become implanted below the top layer of surface atoms or simply scatter from the surface, retaining some fraction of its initial energy.

There have been a series of recent measurements of the trapping probabilities for alkali and reactive ions scattering from metallic surfaces.[1–4] The focus of the work presented here is to compare these measurements to results obtained using classical trajectory simulations. In particular, we compare the measured trapping probabilities of hyperthermal energy O^+ and Na^+ ions scattering from Cu(001) to classical trajectory simulation results. The aim of this work is to obtain a detailed, microscopic understanding of the factors that determine whether or not an incident ion becomes trapped above the top layer of surface atoms. Ultimately, we show that although the trends in the trapping probabilities of O^+ and Na^+ are very different, the measured and calculated trends can be easily understood by considering the *surface corrugation* seen by the incident ions.

There are few previous measurements of trapping probabilities for reactive species scattering from metallic surfaces in the hyperthermal energy regime.[5,6] Kang *et al.*[5] measured the trapping probability of 5–300 eV O^+, C^+, and CO^+ incident on Ni(111) along the surface normal, using Auger electron spectroscopy. The results obtained in their study are similar to those obtained in our recent work,[1] for O^+ incident on Cu(001) along the surface normal. However, in our measurements the angular dependence of the trapping probability has also been investigated. In contrast, there have been several investigations of the trapping of hyperthermal energy alkali ions at metallic surfaces.[3,4,7,8] Hurkmans *et al.*[7,8] have measured the trapping probabilities for Na^+ and K^+ incident on W(110) at energies below 20 eV and for a range of incident angles from 10° to 70°, measured from the surface normal. It was observed that the trapping probability decreased continuously with increasing energy, which qualitatively agrees with the observations made by Goodstein *et al.*[3,4] for Na^+ incident on Cu(001). Furthermore, Hurkmans and co-workers found that the trapping probability was smaller for more grazing incidence scattering geometries. However, the energy range of the measurements performed by Hurkmans *et al.* is significantly lower ($\leqslant$20 eV) than that used in either the Na^+ or O^+ measurements discussed in this paper.[1–4] Finally, there have also been a number of measurements of subsurface implantation during the scattering of noble-gas ions. For example, the bombardment of graphite with He^+, Ne^+, and Ar^+ has been studied by Marton *et al.*[9] at incident energies from 10 to 150 eV and by Choi *et al.*[10] at incident energies from 10 to 600 eV. Since noble-gas atoms do not trap on the surface at room temperature, these studies focused on measuring the energy dependence of subsurface implantation. It was found that subsurface implantation increased as the incident ion energy was increased, which is in general agreement with the results discussed here. For a more complete survey of previous trapping measurements at hyperthermal energies, see Ref. 11. In addition, there is a significant body of literature that addresses surface trapping at thermal energies. For a comprehensive review see Ref. 12 and references therein.

In this work, an ion is considered trapped at the surface if its final location is above the top layer of surface atoms. The probability of this occurring will be referred to as the surface trapping probability, P_S. We distinguish among P_S, the subsurface trapping probability, P_{SS}, (also referred to as implantation), and the total trapping probability, P_T, which is the combined probability of trapping on the surface and subsurface ($P_T = P_S + P_{SS}$). At low incident ion energies, where most of the trapped atoms are expected to be on the surface, P_S and P_T are equivalent. In general, it is expected that P_S will decrease as the incident ion energy is increased since it becomes more difficult for the incident ions to lose sufficient energy to become surface-trapped. On the other hand, P_{SS} is expected to increase with increasing incident ion energy since the ions have more energy to penetrate below the surface. Thus, as the incident ion energy is increased, P_S and P_T will diverge. The exact trends in P_S and P_T will be complex functions of factors such as the interaction potential and the incident angle. As will be seen, these parameters also determine the surface corrugation.

The classical trajectory simulation code[13] used in this study to identify the factors that determine P_S and P_T for the Na^+ and O^+ systems has been applied previously to a wide variety of scattering data and to the trapping measurements for the Na-Cu system.[3] It was possible to make predictions about trapping probabilities for the Na-Cu system using trajectory simulations because a well-known interaction potential was available. The Na-Cu interaction potential used in the simulations has been thoroughly tested by comparison of the simulation results to scattered energy and angular distributions for 10–400 eV Na^+ incident on Cu(001) and Cu(110).[11,14–16] Due to the success of this interaction potential in reproducing such a broad array of measurements, we consider the Na-Cu system to be a *model* system for comparison to the O-Cu system. Before the trajectory simulation could be used to model trapping probabilities in the O-Cu system, it was necessary to calculate an O-Cu interaction potential, the results of which are presented here. It will be seen that by using this potential in the simulation, we can qualitatively reproduce the O data. Typically, scattered ion distributions are used to test calculated ion-surface interaction potentials. However, in some systems, such as the O-Cu system, obtaining scattered spectra is experimentally challenging, and it is important to find an alternative way to test interaction potentials. An important result of this study is that it demonstrates that trapping measurements can provide a sensitive test of hyperthermal energy ion-surface interaction potentials.

The organization of this paper is as follows. In Sec. II we describe the experimental apparatus used to acquire both the O (Refs. 1 and 2) and Na (Refs. 3 and 4) data. In Sec. III we present the experimental results from Refs. 1–4. The classical trajectory simulation code is described in Sec. IV. In Sec. IV A, the details of the calculation of the O-Cu interaction potential are presented, while the results of the simulation for P_S and P_T for the O-Cu and Na-Cu systems are presented in Sec. IV B. The sensitivity of the trapping to variation of the parameters in the interaction potential is given in Sec. IV C. Finally, the failure of an alternative interaction potential, the Ziegler-Biersack-Littmark (ZBL) interaction potential, to reproduce either the O or the Na results is illustrated in Sec. IV D. In the discussion section, Sec. V, we show first, Sec. V A, that the mass difference between Na and O does not explain the differences observed or calculated in the trapping trends. In Sec. V B, we show that it is necessary, instead, to consider the surface corrugation experienced by the incident ions to understand the trapping trends. A microscopic analysis of typical trapping trajectories for the Na-Cu and O-Cu systems is presented along with a demonstration of the effects of modifying the surface corrugation through adjustments in the surface lattice constant. Predictions for future measurements are presented in Sec. VI, and the work is summarized in Sec. VII.

II. EXPERIMENTAL TECHNIQUES

Both the O-Cu and Na-Cu trapping measurements were performed in the same ultrahigh vacuum (UHV) chamber, equipped with a beamline for producing monoenergetic, mass-selected, hyperthermal energy beams in the energy range from 5 eV to 600 eV. This system has been described elsewhere.[17,18] Only the features relevant to the present work are summarized here, with greater emphasis given to the more recent oxygen measurement.

The O^+ ions were extracted from a Colutron ion source[19] using a source gas mixture of 15% O_2–85% Ne, which was enriched with pure O_2 when it was necessary to increase the O^+ ion yield. The solid state source for producing Na^+ beams is described in Ref. 20.

The Cu(001) single crystal was prepared by standard sputter and anneal cycles. Surface cleanliness and long-range order were monitored using Auger electron spectroscopy (AES) and low-energy electron diffraction (LEED), respectively. The base pressure was 3×10^{-11} Torr and operating pressures were below 2×10^{-10} Torr. All beam depositions were performed with the sample at 100 ° C.

Prior to each beam deposition, the incident ion beams were focused into the 1 mm entrance aperture of a Faraday cup located directly below the sample. Each trapping measurement was then performed by exposing the Cu(001) sample to the Na or O beam, incident along the ⟨100⟩ azimuth, for a well-defined amount of time, t. In the low-coverage limit, the resulting spatial distribution on the sample is given by

$$\Theta(\mathbf{r},t)=P_T(E_i,\theta_i)j(\mathbf{r})t\cos(\theta_i). \tag{1}$$

The macroscopic surface coordinate, $\mathbf{r}$, was measured from the center of the profile on the sample. E_i and θ_i are the incident beam energy and angle (measured from the surface normal), and $j(\mathbf{r})$ is the incident ion current density. Cross-sectional profiles of the incident beam currents were measured by sampling the current in the Faraday cup at many positions over a uniform grid. $j(\mathbf{r})$ was obtained from the measured beam current using a numerical deconvolution procedure with Wiener optimized filtering to remove the effect of the finite size of the Faraday cup aperture. The deconvolution procedure was necessary since the width of the incident ion beam was roughly the same as the size of the Faraday cup aperture. Typical beams were roughly Gaussian in shape with ~0.5 mm half-widths.[21–23] Once $j(\mathbf{r})$ had been evaluated, it was necessary to measure $\Theta(\mathbf{r},t)$ to determine the trapping probability using Eq. (1). For incident Na and O beams, $\Theta(\mathbf{r},t)$ was determined using two different methods, described in detail below.

A. Na-Cu

The trapping probabilities measured by Goodstein *et al.*[3,4] for the Na-Cu system were obtained using a technique that relied on charge transfer properties specific to this system. The measurements exploited the fact that the neutralization of scattered Na^+ is highly sensitive to the amount of Na trapped on the top layer of surface atoms. As Na becomes trapped on the surface, the work function decreases rapidly, and, as a result, the neutralization probability increases. By monitoring the intensity of scattered Na^+ ions during the exposure of the sample to the incident Na^+ beam and obtaining the slope of the linearly decreasing intensity, the surface coverage, $\Theta(\mathbf{r},t)$, could be calculated. Since this technique is extremely surface sensitive, it is the surface trapping, P_S,

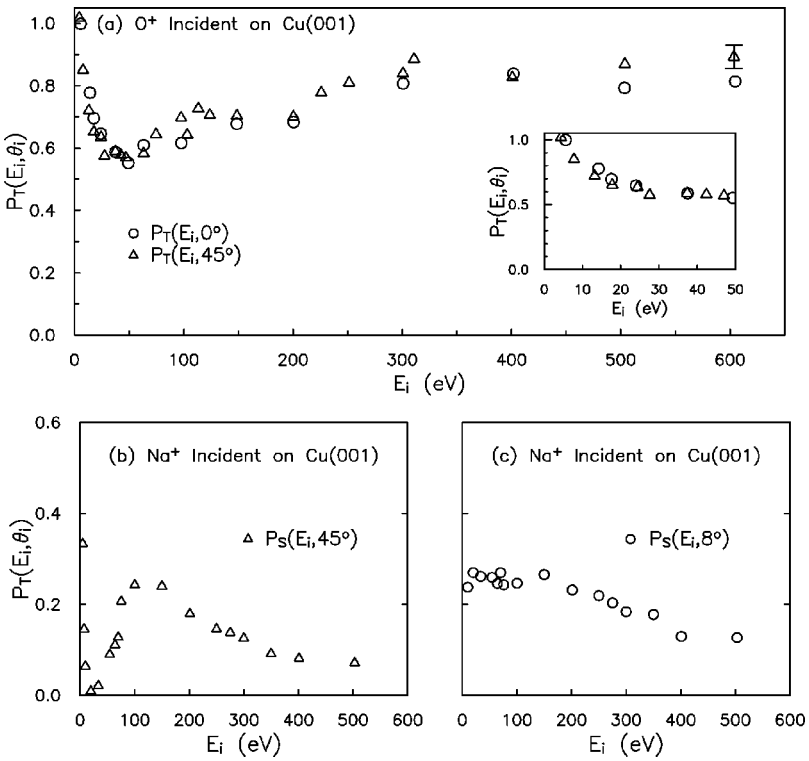

FIG. 1. (a) $P_T(E_i,0°)$ (○) and $P_T(E_i,45°)$ (△) for O^+ incident on Cu(001). Data taken from Refs. 1 and 2. A typical error bar is shown. The inset shows a close up of the low-energy behavior. (b) $P_S(E_i,45°)$ and (c) $P_S(E_i,8°)$ for Na^+ incident on Cu(001). Data taken from Refs. 3 and 4.

and not the total trapping probability, P_T, that is measured. P_S was measured for $\theta_i = 8°$ (i.e., close to normal incidence) and $\theta_i = 45°$.

B. O-Cu

For oxygen, the coverage could not be obtained with the same technique that was used for Na, since the neutralization of hyperthermal energy O^+ on Cu(001) is very high[24] and neutral oxygen is difficult to detect. Furthermore, unlike in the Na-Cu system, the work function change associated with the deposition of oxygen on Cu(001) is small, approximately 200 mV at 100°C, as well as being a complex function of dose.[25,26] Instead, a technique based on AES was developed for measuring $\Theta(\mathbf{r},t)$ for the O-Cu system. To simplify the experimental procedure and minimize the exposure time of the sample to the Auger electron beam, P_T was only evaluated at the center of the oxygen profile on the sample. By performing vertical and horizontal scans across the sample with the Auger spectrometer tuned to the energy of the principal O(503 eV) Auger peak, the center of the profile on the sample was located. The ratio, $R_{\mathrm{O/Cu}}$, of the peak-to-peak heights of the O(503 eV) and Cu(920 eV) Auger signals was then measured at this position. A full Auger scan from 55 eV to 1000 eV was also performed to verify that there was no contamination from other sources. In addition, a second full scan was performed far from the center ($\geqslant$2.5 mm) of the oxygen profile to ensure no measurable level of trapping from background oxygen. $\Theta(\mathbf{r},t)$ was obtained by converting $R_{\mathrm{O/Cu}}$ to an absolute coverage in monolayers (ML). To make this conversion, a separate measurement was performed, in which O_2 was thermally deposited on the Cu(001) sample up to the known saturation coverage $\Theta_{sat} = 0.5$ ML. At saturation coverage, $R_{\mathrm{O/Cu}} = R_{sat} = 0.19$. Thus, for the O-Cu system, P_T is given by

$$P_T(E_i,\theta_i) = \left(\frac{\Theta_{sat}}{R_{sat}}\right)\left(\frac{R_{\mathrm{O/Cu}}(0,t)}{j(0)t\cos(\theta_i)}\right). \tag{2}$$

P_T for the O-Cu system was measured for $\theta_i = 0°$ and $\theta_i = 45°$.

In contrast to the Na-Cu system, measured trapping probabilities for the O-Cu system more accurately represent P_T than P_S, due to typical probing depths of AES (10–30 Å).[27] The interpretation of the O data at energies where subsurface trapping occurs is complicated by the depth-dependent sensitivity of the Auger signal. The Auger signal is more sensitive to surface than to subsurface O since the Auger electrons emitted from the subsurface O are attenuated as they escape the sample.[28] Thus, the conversion of $R_{\mathrm{O/Cu}}$ to absolute coverage is not quantitative once subsurface penetration has become significant.

III. RESULTS

Figure 1 compares the measured trapping probabilities for O^+ and Na^+ scattering from Cu(001). For the O-Cu system, Fig. 1(a), there is little difference between $P_T(E_i,0°)$ and $P_T(E_i,45°)$, although there is a significant dependence on E_i. P_T decreases by almost a factor of two between 5 and 50 eV, while above 50 eV there is a general upward trend. In contrast, for the Na-Cu system, Figs. 1(b) and 1(c), P_S is strongly dependent on θ_i and E_i. $P_S(E_i,8°)$ decreases monotonically with increasing energy while $P_S(E_i,45°)$ is strongly nonmonotonic with a deep minimum at 20–25 eV. This feature is clearly absent in the O data.

The slow increase in P_T above approximately 50 eV, for the O-Cu system, is probably due to the finite probing depth of AES. Although some subsurface penetration is expected to occur below this energy, the results of the classical trajectory simulations indicate that it is not significant at low en-

ergies. Consequently, we are justified in comparing the measurements of P_S for the Na-Cu system to the measurements of P_T for the O-Cu system, at energies below approximately 50 eV.

IV. CLASSICAL TRAJECTORY SIMULATIONS

The classical trajectory simulation code used to model the results for the O and Na trapping probabilities has been described elsewhere,[13] and has successfully reproduced energy and angular spectra for Li^+, Na^+, and K^+ scattering from Cu(001) and Cu(110).[11,14–16,29] Qualitative agreement was also achieved between the results of this simulation and the measurements of P_S performed by Goodstein *et al.*[3,4] for Na^+ trapping on Cu(001).

The classical trajectory simulation code integrates Hamilton's equations of motion for ions interacting with a surface. Use of this sophisticated code is necessary since the incident ions interact with many surface atoms simultaneously, resulting in complex trajectories that cannot be described by a simple binary collision approximation. Determination of trapping probabilities using this code is achieved by calculating the trajectories of a large number of incident ions with impact parameters that are randomly chosen to sample an entire unit cell. Typically, for each incident energy and angle, 10 000 trajectories were calculated, resulting in scattering and surface and subsurface trapping. By summing the number of trajectories that lead to these different outcomes, and knowing the number of impact parameters sampled, P_S, P_{SS}, and P_T, can be calculated. Furthermore, individual trajectories with particular impact parameters can be analyzed, resulting in a microscopic understanding of the trajectory types that lead to trapping.

In these simulations, the criteria used to determine if an incident ion has become trapped on the surface are that the total energy of the ion is negative, the kinetic energy is small ($\leqslant 1$ eV), and the particle is above the top layer of surface atoms. An incident ion is considered trapped subsurface, or implanted, if the total energy is negative and the particle is below the top layer of surface atoms.

The simulations were performed assuming a perfect single crystal Cu(001) surface at zero temperature, in which seven layers of Cu atoms were included. It has been been found previously that calculated trapping probabilities, at the energies we are studying here, are relatively insensitive to the binding forces between the surface atoms or to the effects of thermal vibrations.[3,4]

A. Interaction potentials

A critical component of the classical trajectory simulation code is the ion-surface interaction potential, which has been the subject of many theoretical and experimental investigations.[11,14–16,29–42] In much of this previous work, emphasis has been given to calculating interaction potentials for alkali ions incident on metallic surfaces. There are many reasons for this, including the relative simplicity of detecting scattered alkali ions, the comparatively well understood charge transfer properties, and the noble-gas electronic structure of positive alkali ions, which simplifies the calculation of ion-surface interaction potentials.

The repulsive part of the interaction potential typically used in trajectory simulations is a sum of individual ion–surface-atom pair potentials that model the strong Pauli repulsion that occurs at small separations due to the wave-function overlap of the incident ion and surface atom electrons. Many studies[11,14–16,29–33,42] have also found that to accurately reproduce scattered energy and angular spectra, especially at very low energies, it is necessary to include a long-range attractive term in the interaction potential that models the image charge induced in the metal by the incident ion. Clearly, an attractive term must be included in the interaction potential for there to be any trapping of the incident ions above the top layer of surface atoms. Otherwise, subsurface implantation is the only mechanism by which incident ions can become trapped. Furthermore, this attractive *image* term also serves as a rough model of the chemisorption potential experienced by an incident ion while in the vicinity of the surface.

Throughout this study, the full surface interaction potential is modeled as a sum of repulsive pair potentials, where the sum includes the six Cu surface atoms nearest the incident ion at each point in the trajectory $[\Sigma_{i=1}^{6} V_{pair}(r_i)]$, together with an attractive image term. The repulsive part of the Na-Cu interaction potential has been calculated previously by Goodstein *et al.*[14] and consists of a sum of Hartree-Fock (HF) $[\text{Na-Cu}]^+$ pair potentials.

We have calculated the repulsive $[\text{O-Cu}]^-$ pair potential using the Hartree-Fock code in the quantum chemistry package GAUSSIAN 94.[43] Specifically, the repulsive pair potential, $V_{pair}(r)$, was obtained by calculating the energy of the $[\text{O-Cu}]^-$ triplet (^3P) pair as a function of distance, r, between the O and Cu atom. The energies of the isolated O^- ion and Cu atom were subtracted from the energy of the triplet pair so that $V_{pair}(r) = E([\text{O-Cu}]^-, r) - E(O^-) - E(\text{Cu})$. The parameterization of this pair potential used in the classical trajectory simulation is $V_{pair}(r) = A_1 e^{-B_1 r} + A_2 e^{-B_2 r}$. Figure 2 shows the results of this calculation. For clarity, we will refer to a specific pair potential using the dimer notation from above, e.g., the $[\text{O-Cu}]^-$ repulsive pair potential.

The form of the attractive image potential chosen to model the O-Cu trapping data has also been used in a number of other studies,[11,14–16,31–33,36] and is given by

$$V_{attr}(z) = \begin{cases} \dfrac{-e^2}{\sqrt{16(z-z_0)^2 - e^4/V_{min}^2}} & \text{for} \quad z > z_0 \\ -V_{min} & \text{for} \quad z \leqslant z_0, \end{cases} \tag{3}$$

where z is the perpendicular distance from the top layer of surface atoms. V_{attr} is saturated to V_{min} close to the surface and smoothly tends to $1/4z$ for large values of z. V_{min} and z_0 determine the depth of the image well and are the only adjustable parameters.

The sensitivity of scattered energy and angular spectra to the image potential parameters, V_{min} and z_0, has been investigated for 10–100 eV Na^+ scattering from Cu(001).[11] It was found that the values of V_{min} and z_0 that best reproduced the data were $V_{min} = 2.6$ eV and $z_0 = 0.8$ Å, resulting in a well depth of 1.5 eV. However, well depths in the range from 1.3 eV to 2.6 eV also adequately reproduced the scattered energy

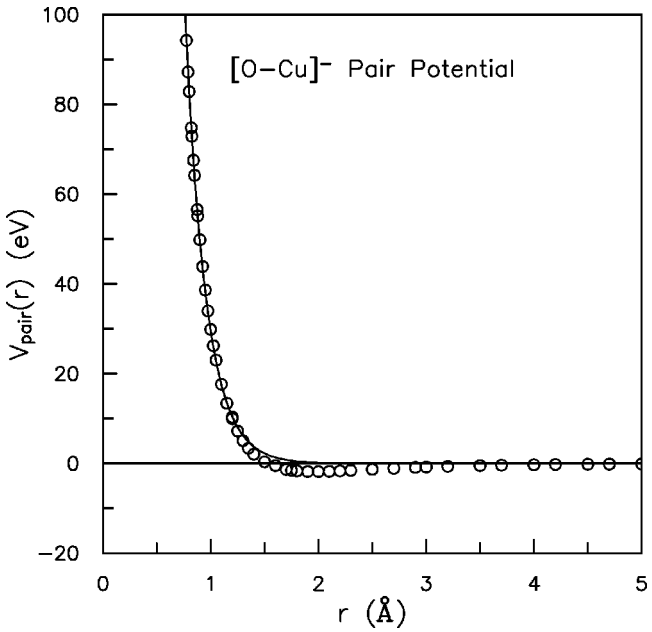

FIG. 2. HF $[O\text{-}Cu]^-$ repulsive pair potential. The solid line is the best fit of $V_{pair}(r)$ to $A_1e^{-B_1r}+A_2e^{-B_2r}$. The best fit values are given by $A_1=2798.2$ eV, $B_1=5.1878$ Å^{-1}, $A_2=2449.5$ eV, and $B_2=5.1770$ Å^{-1}. This potential, together with an image potential given by Eq. (3) with $V_{min}=2.6$ eV and $z_0=0.8$ Å, was used in the classical trajectory simulation to model the trapping of O^+ incident on Cu(001).

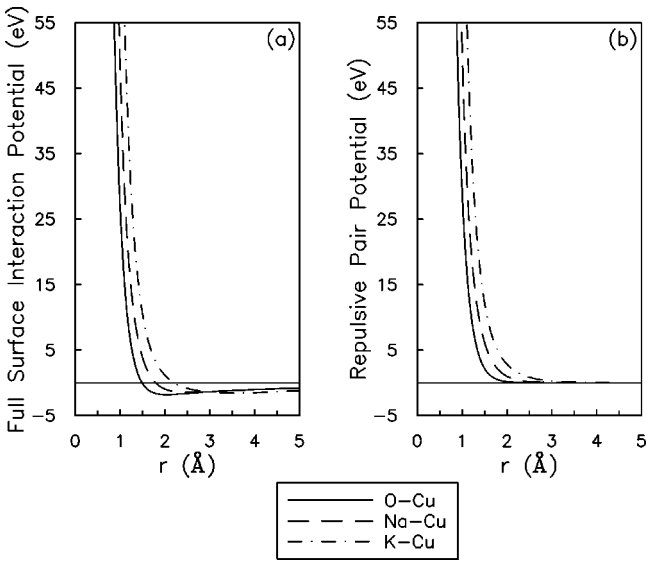

FIG. 3. (a) Full surface O-Cu (solid), Na-Cu (dashed) and K-Cu (dashed-dotted) interaction potentials. The Na-Cu interaction potential was taken from Ref. 11, and the K-Cu interaction potential was taken from Ref. 13. The K-Cu interaction potential is significantly more repulsive than either the O-Cu or Na-Cu interaction potential. (b) Comparison of the HF $[O\text{-}Cu]^-$, $[Na\text{-}Cu]^+$, and $[K\text{-}Cu]^+$ repulsive pair potentials.

and angular distributions. The values of V_{min} and z_0 we chose for the O-Cu interaction potential are the same best-fit values obtained by DiRubio *et al.*[11] for the Na-Cu interaction potential. This corresponds to a well depth of 1.8 eV. As will be seen in the next section, the trapping probabilities for the O-Cu system are not particularly sensitive to the choice of parameters for the image well, within the range of well depth values suggested in Ref. 11.

The full-surface interaction potential for the O-Cu system, obtained by combining the HF $[O\text{-}Cu]^-$ repulsive pair potential and the attractive image term given by Eq. (3), is shown in Fig. 3(a). For comparison, Fig. 3(a) also includes the full-surface interaction potential for the Na-Cu system. Figure 3(b) compares the $[O\text{-}Cu]^-$ and $[Na\text{-}Cu]^+$ pair potentials, from which it can be seen that the $[O\text{-}Cu]^-$ pair potential is significantly less repulsive than the $[Na\text{-}Cu]^+$ pair potential.

The $[O\text{-}Cu]^-$ repulsive pair potential was used instead of the $[O\text{-}Cu]^0$ or $[O\text{-}Cu]^+$ pair potentials because the most energetically favorable charge state of the O-Cu system at small ion-surface separations involves O^-.[24] However, this distinction is relatively unimportant since we have found that the different charge states of the O-Cu dimer result in relatively similar pair potentials.[22] An important point about the classical trajectory simulation code is that the effects of charge transfer are not incorporated into the simulation. Thus, there is no way to include the effects of *changes* in the incident ion charge state.

Finally, in contrast to hyperthermal energy alkali ion scattering from Cu(001), the dominant charge state of the scattered oxygen far from the surface is neutral. Consequently, obtaining energy and angular distributions is complicated by difficulties in detecting low-energy neutral particles. Thus, testing an O-Cu interaction potential by comparison of scattered energy and angular distributions to the results of classical trajectory simulations is challenging. The trapping measurements obtained here provide an alternative method for testing interaction potentials.

B. Results of the classical trajectory simulations

Figure 4(a) shows the results of the classical trajectory simulations for O^+ incident on Cu(001) at $\theta_i=0°$ and $\theta_i=45°$. The results for P_T compare favorably to the data presented in Fig. 1(a), which also showed little variation with θ_i but a large dependence on E_i. P_S also shows little variation with θ_i, decreasing monotonically with increasing energy. Subsurface implantation becomes significant at approximately 40 eV for both incident angles.

The calculated values of P_S and P_T for Na^+ incident on Cu(001) at $\theta_i=0°$ and $\theta=45°$ are shown in Fig. 4(b). The trends in P_S qualitatively reproduce the measurements performed by Goodstein *et al.*[3,4] [Figs. 1(b) and 1(c)]. In particular, $P_S(E_i,0°)$ decreases monotonically with increasing energy while $P_S(E_i,45°)$ is strongly nonmonotonic, decreasing rapidly from large values at 5 eV to close to zero at 20-25 eV, before increasing again to a local maximum at approximately 100 eV. $P_T(E_i,0°)$ diverges quickly from $P_S(E_i,0°)$ for energies above approximately 40–50 eV due to the onset of subsurface implantation. The onset of subsurface implantation at $\theta_i=45°$ occurs at a higher energy, approximately 75 eV, than at normal incidence. The nonmonotonic trend in $P_S(E_i,45°)$ seen in the Na-Cu system is not observed in either the data or the simulations in the O-Cu system.

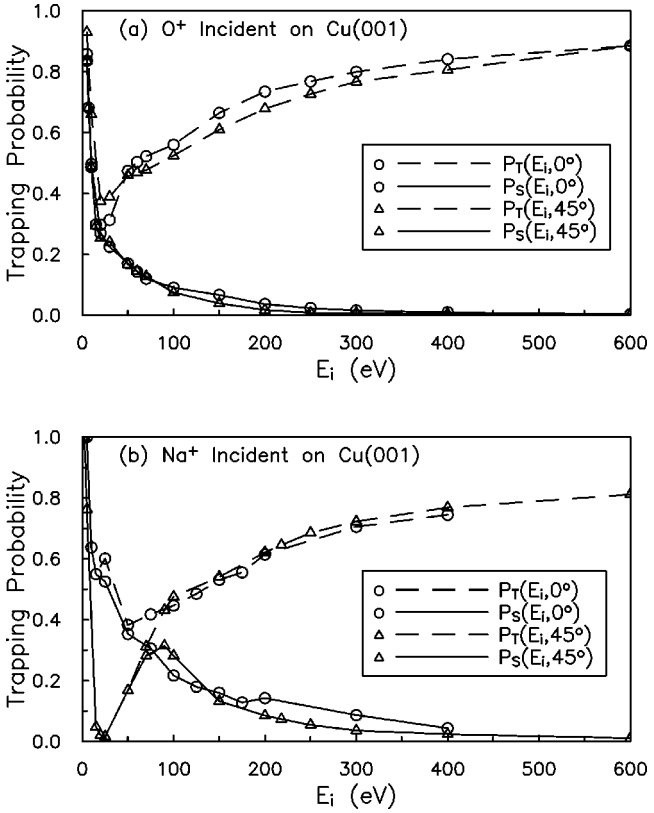

FIG. 4. (a) P_T (dashed lines) and P_S (solid lines) for O^+ incident on Cu(001) at 0° (○) and 45° (△). (b) P_T (dashed lines) and P_S (solid lines) for Na^+ incident on Cu(001) at 0° (○) and 45° (△).

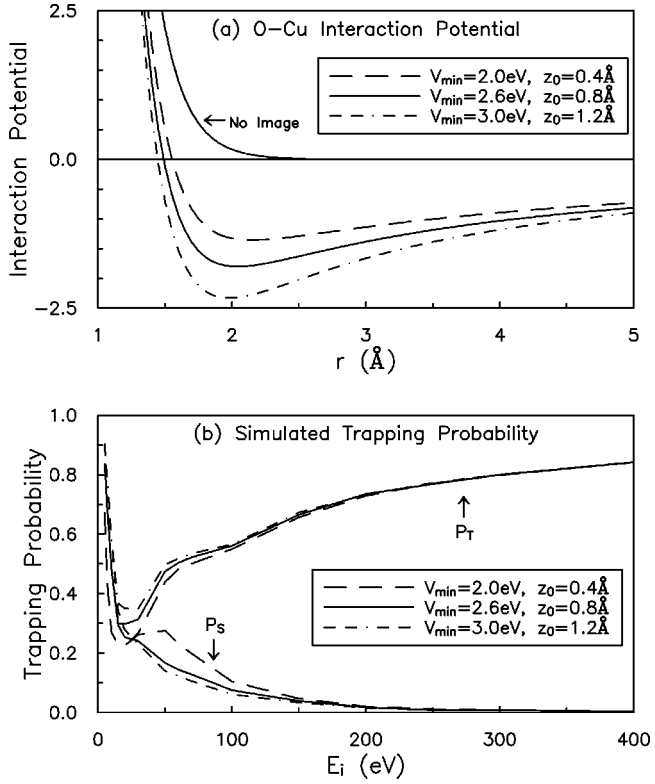

FIG. 5. (a) The full surface O-Cu interaction potential for values of V_{min} and z_0 that vary the well depth from 1.3 eV to 2.5 eV. For comparison, the O-Cu interaction potential without the image potential is also shown. (b) $P_S(E_i,45°)$ and $P_T(E_i,45°)$ for O^+ incident on Cu(001) for the different image parameterizations shown in (a). There is no surface trapping if the image potential is not included (not shown in figure).

C. Sensitivity to image parameters

The sensitivity of P_S and P_T to the parameterization of the image potential was determined by varying V_{min} and z_0 so as to keep the total depth of the potential well within the range of 1.3 eV to 2.6 eV, as suggested in Ref. 11. Figure 5(a) shows the O-Cu interaction potential for various combinations of V_{min} and z_0 that span this range of well depths. $P_S(E_i,45°)$ and $P_T(E_i,45°)$, calculated using the different combinations of V_{min} and z_0, are shown in Fig. 5(b) and do not change significantly for the range of well depths probed. For the shallowest well depth, approximately 1.3 eV, corresponding to $V_{min}=2.0$ eV and $z_0=0.4$ Å, a slightly nonmonotonic trend in $P_S(E_i,45°)$ has developed. However, the differences between $P_S(E_i,45°)$ and $P_T(E_i,45°)$ for the different image potential parameterizations are small, and in all cases the agreement with the data is reasonable.

D. Comparison of HF and ZBL interaction potentials

To illustrate that the results of the simulation are sensitive to the choice of repulsive pair potential, we also used the universal Ziegler-Biersack-Littmark (ZBL) pair potential[40] to model the repulsive part of the O-Cu interaction potential. The ZBL pair potential depends only on the atomic numbers of the projectile and target atoms and not on the charge of the projectile-target dimer. ZBL potentials have been used to successfully describe the scattering of Li^+, Na^+, and K^+ from Mo(001) in the much higher energy regime[41] from 500 eV to 2500 eV and are consequently a possible choice for use here. However, we will show that our simulations using a ZBL potential do not reproduce the qualitative behavior of P_T for 5–600 eV O^+ trapping on Cu(001). Similarly, though the results are not presented here, we have found that the Na-Cu ZBL potential does not reproduce P_S or P_T for 5–600 eV Na^+ trapping on Cu(001).

Figure 6(a) illustrates that the ZBL O-Cu pair potential is considerably more repulsive than the $[O\text{-}Cu]^-$ HF pair potential. This leads to large differences in the trapping probabilities for O^+ scattering from Cu(001) as can be seen in Fig. 6(b). When the ZBL interaction potential is used there is no surface trapping or implantation for the range of incident ion energies from 15 eV to approximately 85 eV. Furthermore, subsurface implantation occurs at a much higher incident ion energy, at approximately 115 eV. Both these observations are a direct consequence of the fact that the ZBL interaction potential is more repulsive, leading to a less corrugated surface and hence to lower surface trapping (see Sec. V) as well as more energy being required to penetrate below the surface and implant.

The image parameters ($V_{min}=3.2$ eV, $z_0=1.3$ Å) used to obtain the full O-Cu ZBL interaction potential were adjusted so as to give a well depth similar to that used in the full O-Cu HF interaction potential. The motivation for this was that adding the same image potential to dissimilar repulsive pair potentials results in attractive wells of different depths, which is expected to affect the overall amount of

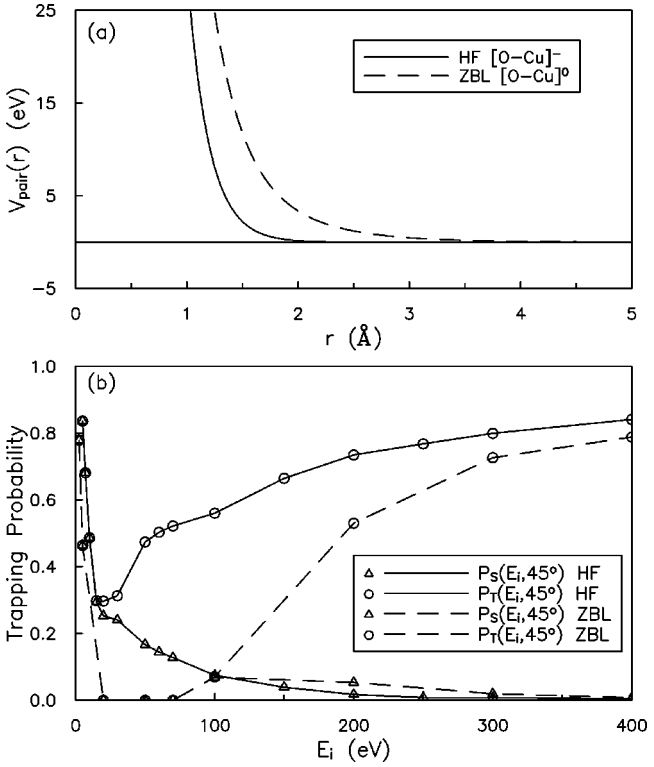

FIG. 6. (a) Comparison of HF $[\text{O-Cu}]^-$ (solid line) and O-Cu ZBL (dashed line) repulsive pair potentials. (b) Comparison of $P_S(E_i,45°)$ ($\triangle$) and $P_T(E_i,45°)$ ($\bigcirc$) for O-Cu using the HF (solid line) and ZBL (dashed line) potentials.

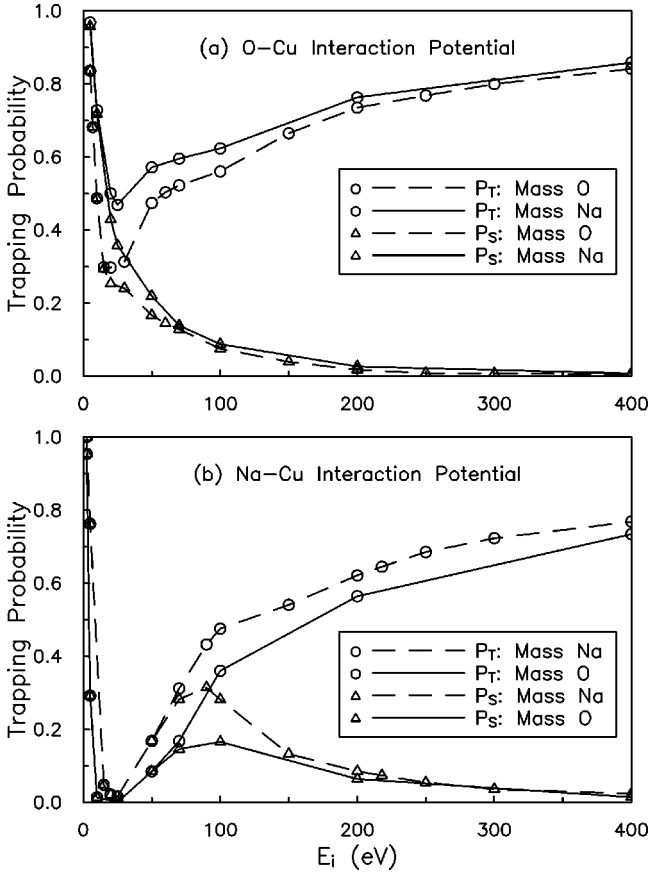

FIG. 7. (a) Comparison of $P_T(E_i,45°)$ ($\bigcirc$) and $P_S(E_i,45°)$ ($\triangle$) for O^+ incident on Cu(001), calculated using the O-Cu HF interaction potential with the correct mass for O (dashed line) and with the mass of Na (solid line). (b) Comparison of $P_T(E_i,45°)$ ($\bigcirc$) and $P_S(E_i,45°)$ ($\triangle$) for Na^+ incident on Cu(001), calculated using the Na-Cu HF interaction potential with the correct mass for Na (dashed line) and with the mass of O (solid line).

trapping. However, different values of the image parameters were tested and none of the conclusions drawn is significantly affected. Shallower image wells simply resulted in lower trapping probabilities, while the general trends remained unchanged.

V. DISCUSSION

In this section we develop a general understanding of the microscopic parameters important in determining trapping trends and discuss the factors that must be considered to explain the differences observed in the Na-Cu and O-Cu systems. We will pay particular attention to the $\theta_i = 45°$ scattering geometry, since this is where the differences between the two systems are most evident.

A. Mass difference between Na and O

One obvious consideration when comparing the Na-Cu and O-Cu systems is the mass difference between Na and O, since the energy transfer that occurs in collisions will be different due to the dissimilar masses. By interchanging the Na and O masses in the trajectory simulation, we can demonstrate that this change in energy transfer is not the source of the dissimilar trapping probabilities shown in Fig. 1.

This is illustrated in Fig. 7 where $P_S(E_i,45°)$ and $P_T(E_i,45°)$ have been calculated with the masses of O and Na interchanged. First, using the O-Cu interaction potential, we have calculated $P_S(E_i,45°)$ and $P_T(E_i,45°)$ using both the Na and O masses. These results are compared in Fig. 7(a), and it is clear that the values obtained are very similar. One difference, however, is that the trapping probabilities are slightly larger when the mass of Na is used. This is reasonable since the larger Na mass results in a larger energy loss and, consequently, a higher probability of being trapped. Similarly, using the Na-Cu interaction potential, $P_S(E_i,45°)$ and $P_T(E_i,45°)$ have been calculated using both the Na and O masses. Once again, the calculated trends in P_S and P_T are very similar. In particular, the nonmonotonic trend in P_S is reproduced. However, the rise in P_S above 20–25 eV is diminished in magnitude when the mass of O is used. This is understandable, since the smaller O mass leads to a smaller energy loss and a lower probability of being trapped in the attractive well close to the surface.

It is clear from these results that the trapping trends are not significantly altered when the masses are interchanged. Instead, the masses merely have a slight affect on the overall magnitude of the trapping. The general trends in the trapping appear to be more dependent on the choice of interaction potential. This dependence, which is intrinsically related to the choice of incident and surface species, can be incorporated into the concept of surface corrugation, discussed in the next section.

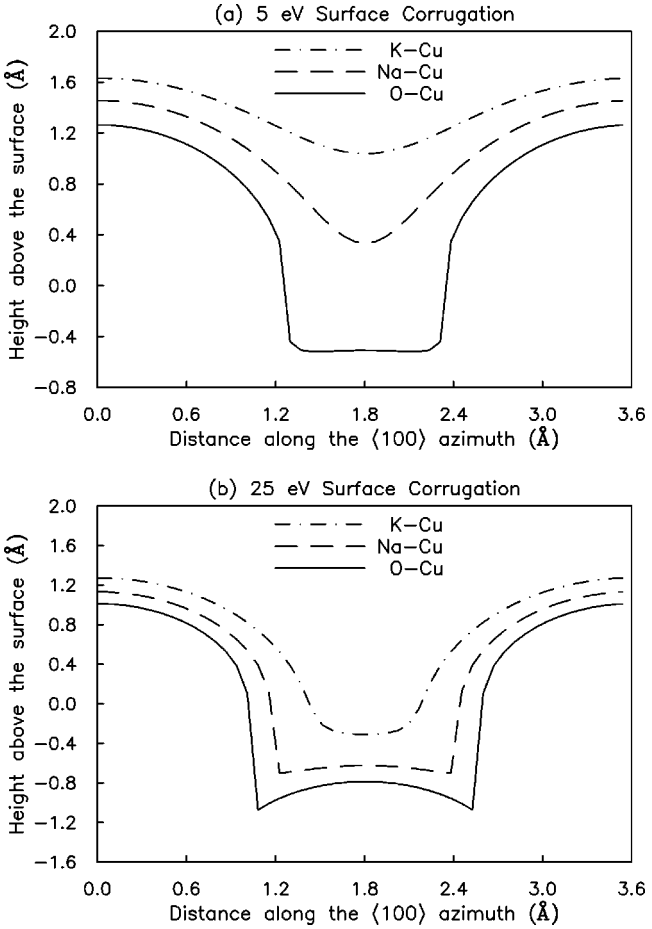

FIG. 8. (a) Comparison of the surface corrugation seen by 5 eV O^+ (solid line), Na^+ (dashed line), and K^+ (dashed-dotted line) incident on Cu(001) along the ⟨100⟩ azimuth. (b) Comparison of the surface corrugation seen by 25 eV O^+ (solid line), Na^+ (dashed line), and K^+ (dashed-dotted line) incident on Cu(001) along the ⟨100⟩ azimuth.

B. Surface corrugation

The surface corrugation can be thought of as the combination of the many factors that affect the trajectory followed by an incident ion with a given impact parameter. These factors include the incident ion species, the surface species and structure, and the incident ion energy and angle. For an ion incident at a particular energy, the surface corrugation can be represented by an equipotential surface of the same energy as that of the incident ion. This equipotential surface is the *initial* corrugation seen by the incident ion. However, at angles other than normal incidence, it is an overestimation of the surface corrugation since the effect of the incident angle has not been taken into account. Furthermore, once the incident ion interacts with the surface, it loses some fraction of its initial energy, and the equipotential surface it is probing changes. As we will proceed to show, though, the differences in the initial corrugation without accounting fully for the incident angle, are sufficient to explain the observed trapping trends.

Figure 8(a) shows slices through 5 eV equipotential surfaces for Na^+ and O^+ ions incident on Cu(001) along the ⟨100⟩ azimuth. It can be seen that the surface corrugation for a 5 eV O^+ ion is significantly larger than that for a 5 eV Na^+ ion. In fact, the surface is more corrugated at all incident energies for O^+ than Na^+ since the $[O\text{-}Cu]^-$ pair potential is less repulsive than the $[Na\text{-}Cu]^+$ pair potential [see Fig. 3(b)]. Figure 8(b) shows equipotential surfaces for 25 eV Na^+ and O^+ ions incident on Cu(001) along the ⟨100⟩ azimuth. It is clear that for a given incident ion the surface corrugation increases as the incident energy of the ion is increased.

Incorporating the effect of incident angle on the surface corrugation is a more complex problem. However, a qualitative understanding of the effects of incident angle can be obtained by considering a fixed incident ion energy and equipotential surface. As the incident angle is made to be more grazing, a larger fraction of the surface will be blocked from direct collisions by incident particles. In other words, at scattering geometries with a more grazing angle of incidence, the surface appears ''flatter'' or less corrugated. In the limit that θ_i approaches 90°, the apparent surface corrugation completely disappears. Similarly, the surface appears more open at the most normal incident angles.

In order to demonstrate the importance of the surface corrugation in determining the trapping trends in the Na-Cu and O-Cu systems, we have performed a detailed trajectory analysis. This analysis, described below, has revealed distinct trajectory types that can be classified according to the surface corrugation. Furthermore, we have studied the dependence of the trapping probabilities on changes in the lattice constant.

1. Trajectory analysis

Trajectory analysis has shown that the trajectory types that lead to *surface* trapping can be classified into two general types: low-corrugation (LC) and high-corrugation (HC) trajectory types. LC trajectory types occur when the corrugation is small and are relatively simple trajectories in which the incident ions do not penetrate very deeply below the first layer of surface atoms. These trajectories typically involve collisions in which the incident ions do not lose a very large fraction of their incident energy. HC trajectory types occur when the surface corrugation is larger. For these trajectories, incident ions penetrate deeper below the surface, typically below the first layer of surface atoms, and are involved in multiple large-angle collisions where a larger fraction of the incident energy is lost.

Figure 9 shows representative trajectories that lead to surface trapping for Na^+ and O^+ incident at 5 eV and 50 eV. This figure illustrates the differences between archetypal LC and HC trajectory types. For clarity, the trajectories shown in Fig. 9 were chosen with impact parameters on a row of surface Cu atoms along the ⟨100⟩ azimuth. This choice constrains the trajectories to lie on the plane containing the surface normal and the ⟨100⟩ azimuth. Trajectories with impact parameters that are not along this high-symmetry chain are found to have the same general properties as those shown in Fig. 9.

By categorizing trajectories as either LC or HC, we can explain many of the trapping trends observed in the Na-Cu and O-Cu systems. Our basic approach involves determining the energy ranges, for a given incident angle, over which the different trajectory types occur.

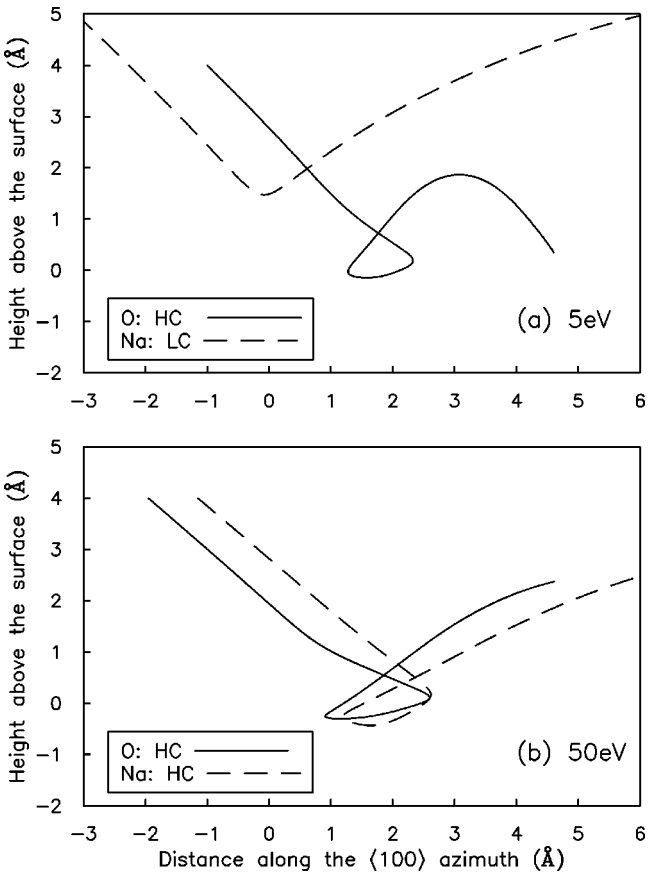

FIG. 9. Typical trapping trajectories for (a) 5 eV and (b) 50 eV O^+ (solid lines) and Na^+ (dashed lines) incident on Cu(001) along the ⟨100⟩ azimuth at $\theta_i = 45°$.

For Na^+ scattering from Cu(001), trajectory analysis has revealed that below 25 eV, most of the trajectories contributing to $P_S(E_i,45°)$ are of the LC type [Fig. 9(a)]. Recalling that $P_S(E_i,45°)$ is highly nonmonotonic with a deep minimum at 20–25 eV (Figs. 1 and 4), we can see that the initial decrease in $P_S(E_i,45°)$ between 5 eV and 25 eV follows a trend that is consistent with a simple energy transfer argument. Specifically, since the LC trajectory type is dominant in this energy range, $P_S(E_i,45°)$ decreases as the incident energy is increased because it becomes more difficult for incident ions to lose enough energy to become trapped. At 25 eV, the surface corrugation has increased sufficiently to allow the HC trajectory type to turn-on [Fig. 9(b)], and as the incident ion energy is increased above 25 eV, the HC trajectory type dominates. Since this trajectory type transfers more energy to the surface, more of the incident ions lose enough energy to become trapped, and $P_S(E_i,45°)$ increases above 25 eV. As E_i is increased above 100 eV, $P_S(E_i,45°)$ decreases due to the onset of subsurface implantation. Extending these arguments to the $\theta_i = 0°$ geometry, we recall that the surface corrugation will increase as the incident angle becomes more normal. Therefore, the surface corrugation at $\theta_i = 0°$ is larger than at $\theta_i = 45°$, and the HC trajectory types appear at lower energies. In fact, trajectory analysis reveals that at $\theta_i = 0°$ HC trajectories occur at incident ion energies as low as 5 eV. So, in contrast to $\theta_i = 45°$, where there was a relatively sharp transition at 25 eV from the LC to the HC trajectory type, HC trajectory types occur over the entire energy range at $\theta_i = 0°$. This leads to the constant decrease observed in $P_S(E_i,0°)$ with increasing incident ion energy.

Turning now to the O-Cu system, we recall that there was little angular dependence observed in the trapping probabilities (Figs. 1 and 4). Furthermore, since the surface corrugation seen by incident O^+ ions is significantly larger than that seen by incident Na^+ ions (Fig. 8), it is not surprising that trajectory analysis reveals that the HC trajectory types occur over the entire energy range studied. This is true for O^+ incident at $\theta_i = 0°$ and at $\theta_i = 45°$ and is very similar to the case of Na^+ incident at $\theta_i = 0°$ described above. Consequently, P_S decreases monotonically with incident ion energy for O^+ incident at both 0° and at 45°, much like P_S for normal incidence Na^+. The turn-on of subsurface implantation observed in the O-Cu system occurs since a more corrugated surface is more open, and the incident ions can penetrate below the surface at lower incident ion energies.

In summary, our results have revealed that the surface corrugation determines which trajectory types will contribute to P_S at a given incident ion energy and angle. As a result of the large surface corrugation in the O-Cu system, the HC trajectory type contributes to P_S over the entire energy range studied at both $\theta_i = 0°$ and $\theta_i = 45°$. This is similar to Na^+ incident at $\theta_i = 0°$, where the surface corrugation is sufficiently large such that HC trajectory types also occur over the entire energy range. For Na^+ incident at $\theta_i = 45°$, however, the surface corrugation at low incident ion energies is not large enough to allow HC trajectory types to occur, and only LC trajectory types contribute to P_S. The surface corrugation increases as the incident ion energy is increased above 25 eV, and HC trajectory types begin to contribute to P_S. Therefore, we see that for the case of Na^+ incident on Cu(001) at $\theta_i = 45°$, the parameters that determine the surface corrugation combine in a unique way such that there is a distinct separation between the LC and HC trajectory types at 20–25 eV, which gives rise to the observed minimum in P_S.

2. Adjusting the lattice constant

To investigate the importance of the Cu(001) surface structure in determining the corrugation seen by the incident ions, we have varied the lattice constant in our trajectory simulations. Clearly, the face-centered-cubic structure of Cu(001), with a lattice constant of 3.61 Å, plays a critical role in determining the surface corrugation. We have increased the surface lattice constant such that the surface corrugation seen by Na^+ incident on the modified surface closely resembles the surface corrugation seen by O^+ ions incident on the real Cu(001) surface. This was done by increasing the lattice constant to 4.0 Å.

Figure 10(a) compares the 5 eV equipotential surface seen by O^+ incident on the Cu(001) surface with the correct lattice constant to that seen by Na^+ incident on the modified Cu(001) surface. It is clear that this increase in the lattice constant has made the surface corrugation seen by the incident O^+ and Na^+ ions very similar. Figure 10(b) shows $P_S(E_i,45°)$ and $P_T(E_i,45°)$ for Na^+ incident on the modified Cu(001) surface. For comparison, $P_S(E_i,45°)$ and

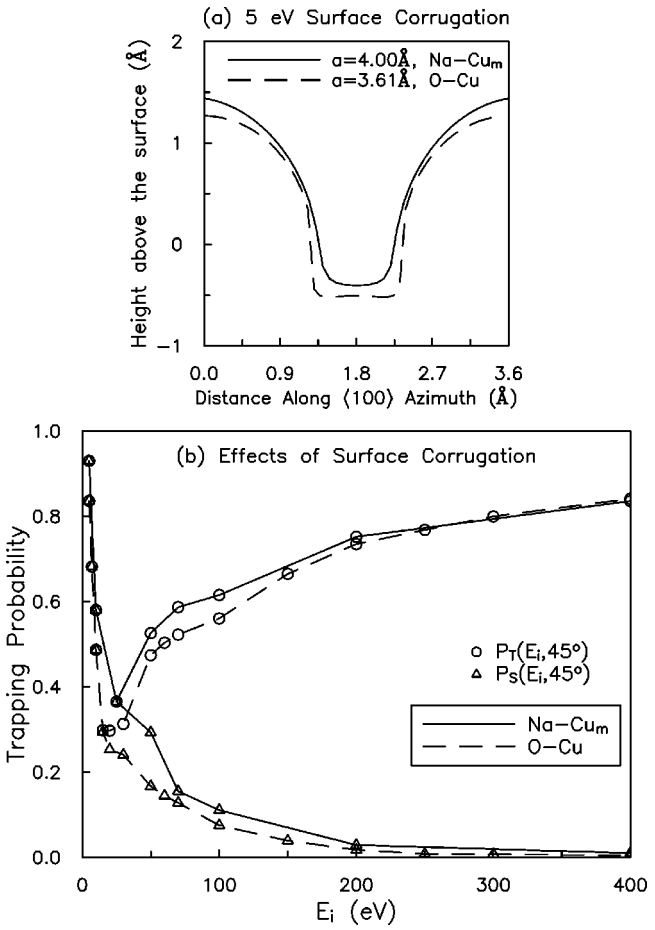

FIG. 10. (a) Cross section through 5 eV equipotential surfaces for O^+ and Na^+ incident on Cu(001) with lattice constant values of 3.61 Å and 4.0 Å, respectively. (b) Comparison of $P_S(E_i,45°)$ (△) and $P_T(E_i,45°)$ (○) for O^+ and Na^+ incident on Cu(001) with lattice constant values of 3.61 Å (dashed line) and 4.0 Å (solid line), respectively. Cu_m refers to the modified Cu(001) surface with the larger lattice constant of 4.0 Å.

$P_T(E_i,45°)$ for O^+ incident on the Cu(001) surface with the correct lattice constant are also included in this figure. The trends in both P_S and P_T are now very similar, and in particular, the nonmonotonic trend in $P_S(E_i,45°)$ for the incident Na^+ ions has completely vanished. In other words, by increasing the surface lattice constant we have destroyed the unique combination of parameters that gave rise to the ''trademark'' nonmonotonic behavior in $P_S(E_i,45°)$ for Na^+.

This result, which shows that the simulated trends in the surface trapping probabilities are sensitive to 20% changes in the lattice constant of Cu(001), also provides further evidence that the surface corrugation is critical in determining the trapping trends. With this sensitivity, measurements of trapping probabilities may provide a stringent test of ion-surface interaction potentials.

VI. PREDICTIONS

Using the classical trajectory simulation and the K-Cu interaction potential determined in Ref. 13 predictions can be made about the trapping probability of K^+ incident on Cu(001). The K-Cu interaction potential used in these simulations has been successfully tested against scattered energy and angular spectra for 100-400 eV K^+ incident on Cu(110). The repulsive part of the interaction potential consists of a sum of HF $[K\text{-}Cu]^+$ pair potentials, and the attractive image potential parameters were set to be $V_{min}=3.0$ eV and $z_0=1.7$ Å. It is clear from Fig. 3 that the $[K\text{-}Cu]^+$ pair potential is significantly more repulsive than either the $[O\text{-}Cu]^-$ or $[Na\text{-}Cu]^+$ pair potentials. Thus, for a given incident energy and angle, K^+ ions will experience a smaller surface corrugation than incident Na^+ or O^+ ions. This is illustrated in Fig. 8, where slices through the Cu(001)⟨100⟩ 5 eV equipotential surfaces for K-Cu, Na-Cu, and O-Cu are compared.

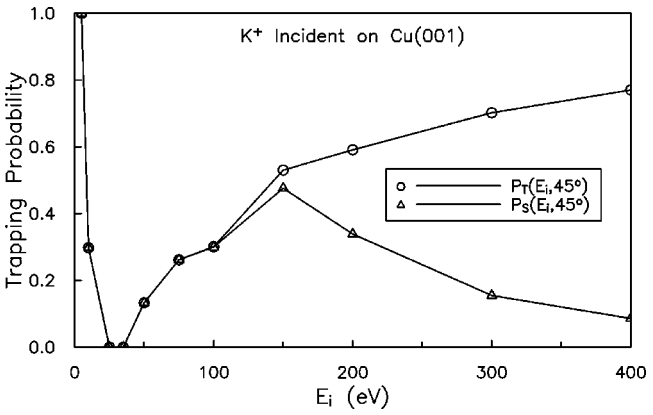

FIG. 11. $P_S(E_i,45°)$ (△) and $P_T(E_i,45°)$ (○) for K^+ incident on Cu(001).

Figure 11 shows the predicted trends in $P_S(E_i,45°)$ and $P_T(E_i,45°)$ for K^+ incident on Cu(001). It can be seen that P_S is highly nonmonotonic, with a deep minimum in which P_S and P_T fall to zero for the range of energies from 30–40 eV. The rise in P_S above 40 eV is very pronounced, and P_S reaches a sizable maximum before decreasing again due to an increase in subsurface implantation. Furthermore, P_T does not diverge from P_S until approximately 150 eV. Trajectory analysis has shown that below the minimum in P_S all trajectories are of the LC type, while above the minimum in P_S, HC trajectory types dominate. Thus, as in the Na-Cu system at $\theta_i=45°$, there is a distinct separation in the range of energies over which the HC and LC trajectory types occur. Measurement of a deep minimum in the surface trapping probability for the K-Cu system would provide additional evidence of the importance of surface corrugation in determining trapping probabilities in the hyperthermal energy regime.

VII. CONCLUSIONS

Classical trajectory simulations have been used to model the trapping probabilities of hyperthermal energy O^+ and Na^+ ions scattering from a Cu(001) surface. Excellent qualitative agreement between the results of these simulations and measured trapping probabilities for O^+ and Na^+ scattering from Cu(001) have been found.[1–4] Through careful analysis of the different trajectory types that lead to surface trapping, we have been able to develop a microscopic understanding of trapping mechanisms.

We have found that, in general, trapping probabilities are highly sensitive to the surface corrugation seen by the incident ions, which is determined by the ion-surface interaction potential and the incident ion energy and angle. Trajectory analysis of the O-Cu and Na-Cu systems has shown that there are two general types of trajectories, dependent on the surface corrugation, that lead to surface trapping. High-corrugation trajectory types dominate when the surface corrugation is large and low-corrugation trajectory types dominate when the surface corrugation is small. Trends in the trapping probabilities can be explained in terms of the range of energies over which these different trajectory types occur. For incident O^+ ions it has been determined that the surface corrugation seen at a given incident ion energy is significantly higher than that seen by incident Na^+ ions. This difference can be attributed to the $[O\text{-}Cu]^-$ pair potential being less repulsive than the $[Na\text{-}Cu]^+$ pair potential. As a result, high-corrugation trajectory types occur over the entire range of incident ion energies for O^+ ions scattering from Cu(001) at both $\theta_i = 0°$ and $\theta_i = 45°$. In contrast, for the Na-Cu system at $\theta_i = 45°$, there is a sharp separation at approximately 25 eV between the low-corrugation and high-corrugation trajectory types. For the Na-Cu system at $\theta_i = 0°$, the high-corrugation trajectory types occur over the entire range of incident ion energies. Thus the angular dependence of the trapping probabilities for the Na-Cu system, as well as the differences between the Na-Cu and O-Cu system at $\theta_i = 45°$, can be explained by the trajectory types allowed by the surface corrugation.

To further establish the importance of the surface corrugation in determining trapping trends, the surface corrugation was modified in the simulation by adjusting the lattice constant of the surface. By increasing the Cu(001) lattice constant, the surface corrugation was increased, and the nonmonotonic trend in the surface trapping for Na^+ incident on Cu(001) at $\theta_i = 45°$ was eliminated.

From these results, we can conclude that for systems with low surface corrugation, changes in the incident angle can have very large effects on the surface trapping probability. This was the case for the Na-Cu system. When the surface corrugation is sufficiently high, changes in the incident angle do not have a large effect on the surface trapping probability, as was observed in the O-Cu system.

ACKNOWLEDGMENTS

The authors would like to thank G.V. Chester for assisting with the preparation of this manuscript. This work was supported by the National Science Foundation (NSF-DMR-9722771), C.E.S. was supported individually by the NSF, and this research was conducted using the resources of the Cornell Theory Center.

*Recently deceased.

[1] A. C. Lavery, C. E. Sosolik, and B. H. Cooper, Phys. Rev. Lett. **83**, 5286 (2000).

[2] A. C. Lavery, C. E. Sosolik, and B. H. Cooper, Nucl. Instrum. Methods Phys. Res. B **157**, 214 (1999).

[3] D. M. Goodstein, E. B. Dahl, C. A. DiRubio, and B. H. Cooper, Phys. Rev. Lett. **78**, 3213 (1997).

[4] E. B. Dahl, D. M. Goodstein, C. A. DiRubio, and B. H. Cooper, Nucl. Instrum. Methods Phys. Res. B **125**, 237 (1997).

[5] H. Kang, S. R. Kasi, and J. W. Rabalais, J. Chem. Phys. **88**, 5882 (1988).

[6] H. Akazawa and Y. Murata, J. Chem. Phys. **92**, 5551 (1990).

[7] A. Hurkmans, E. G. Overbosch, and J. Los, Surf. Sci. **59**, 488 (1976); **62**, 621 (1977).

[8] A. Hurkmans, E. G. Overbosch, D. R. Olander, and J. Los, Surf. Sci. **54**, 154 (1976).

[9] D. Marton, K. J. Boyd, T. Lytle, and J. W. Rabalais, Phys. Rev. B **48**, 6757 (1993).

[10] W. Choi, C. Kim, and H. Kang, Surf. Sci. **281**, 323 (1993).

[11] C. A. DiRubio, R. L. McEachern, J. G. McLean, and B. H. Cooper, Phys. Rev. B **54**, 8862 (1996).

[12] C. R. Arumainayagam and R. J. Madix, Prog. Surf. Sci. **38**, 1 (1991).

[13] D. M. Goodstein, S. A. Langer, and B. H. Cooper, J. Vac. Sci. Technol. A **6**, 703 (1988).

[14] D. M. Goodstein, R. L. McEachern, and B. H. Cooper, Phys. Rev. B **39**, 13 129 (1989).

[15] R. L. McEachern, D. M. Goodstein, and B. H. Cooper, Phys. Rev. B **39**, 10 503 (1989).

[16] D. L. Adler and B. H. Cooper, Phys. Rev. B **43**, 3876 (1991).

[17] R. L. McEachern, D. L. Adler, D. M. Goodstein, G. A. Kimmel, B. R. Litt, D. R. Peale, and B. H. Cooper, Rev. Sci. Instrum. **59**, 2560 (1988).

[18] D. L. Adler and B. H. Cooper, Rev. Sci. Instrum. **59**, 137 (1988).

[19] M. Menzinger and L. Wåhlin, Rev. Sci. Instrum. **40**, 102 (1969).

[20] D. R. Peale, D. L. Adler, B. R. Litt, and B. H. Cooper, Rev. Sci. Instrum. **60**, 730 (1989).

[21] E. B. Dahl, Ph.D. thesis, Cornell University, 1998.

[22] A. C. Lavery, Ph.D. thesis, Cornell University, 1999.

[23] C. E. Sosolik, A. C. Lavery, E. B. Dahl, and B. H. Cooper, Rev. Sci. Instrum. **71**, 3326 (2000).

[24] A. C. Lavery, C. E. Sosolik, and B. H. Cooper, Phys. Rev. B **61**, 2291 (2000).

[25] P. Hofmann, R. Unwin, W. Wyrobisch, and A. M. Bradshaw, Surf. Sci. **72**, 635 (1978).

[26] C. Benndorf, B. Egert, G. Keller, H. Seidel, and F. Thieme, J. Phys. Chem. Solids **40**, 877 (1979).

[27] D. Briggs and M. P. Seah, *Practical Surface Analysis* (Wiley, Chichester, England, 1990).

[28] O. Millo, A. Many, and Y. Goldstein, J. Vac. Sci. Technol. A **7**, 2688 (1989).

[29] E. R. Behringer, J. G. McLean, and B. H. Cooper, Phys. Rev. B **53**, 7510 (1996).

[30] E. Hulpke, Surf. Sci. **52**, 615 (1975).

[31] E. Hulpke and K. Mann, Surf. Sci. **133**, 171 (1983).

[32] A. D. Tenner, R. P. Saxon, K. T. Gillen, D. E. Harrison, T. C. M. Horn, and A. W. Kleyn, Surf. Sci. **172**, 121 (1986).

[33] A. D. Tenner, K. T. Gillen, T. C. M. Horn, J. Los, and A. W. Kleyn, Surf. Sci. **172**, 90 (1986).

[34] A. D. Tenner, K. T. Gillen, T. C. M. Horn, J. Los, and A. W. Kleyn, Phys. Rev. Lett. **52**, 2183 (1984).

[35] P. J. van den Hoek, A. D. Tenner, A. W. Kleyn, and E. J. Baerends, Phys. Rev. B **34**, 5030 (1986).

[36] P. J. van den Hoek and A. W. Kleyn, J. Chem. Phys. **91**, 4318 (1989).

[37] P. J. van den Hoek, T. C. M. Horn, and A. W. Kleyn, Surf. Sci. **198**, L335 (1988).
[38] P. H. F. Reijnen, P. J. van den Hoek, A. W. Kleyn, U. Imke, and K. J. Snowdon, Surf. Sci. **221**, 427 (1989).
[39] T. C. M. Horn, Pan Haochang, P. J. van den Hoek, and A. W. Kleyn, Surf. Sci. **201**, 573 (1988).
[40] P. Biersack and J. F. Ziegler, in *Ion Implantation Techniques*, edited by H. Ryssel and H. Glawischnig, Springer Series in Electrophysics Vol. 10 (Springer-Verlag, Berlin, 1982).
[41] S. H. Overbury and D. R. Huntley, Phys. Rev. B **32**, 6278 (1985).
[42] S. R. Kasi, M. A. Kilburn, H. Kang, J. W. Rabalais, L. Tavernini, and P. Hochmann, J. Chem. Phys. **88**, 5902 (1988).
[43] M. J. Frisch *et al.*, *Gaussian 94* (Gaussian, Pittsburgh, 1994).